Published by
NIGERIAN SOCIETY OF PHYSICAL SCIENCES
Available online @ https://journal.nsps.org.ng/index.php/jnsps

Journal Logo

J. Nig. Soc. Phys. Sci. 6 (2024) 2148

Sonochemical synthesis, characterization, and ADMET studies of Fe (II) and Cu (II) nano-sized complexes of trimethoprim

B. C. Asogwa*, O. M. Mac-kalunta, J. I. Iheanyichukwu, I. E. Otuokere, K. Nnochirionye

Department of Chemistry, Michael Okpara University of Agriculture Umudike, Abia State

Abstract

Nanoparticles exhibit distinct physical and chemical characteristics and are becoming increasingly significant in the production of innovative nanodevices for many applications in physics, biology, biomedicine, and pharmaceuticals. The aim of this research work is to synthesize Fe (II) and Cu (II) nano-sized complexes of trimethoprim (TMP) using the sonication method, characterize them using physical and spectroscopic methods, and carry out ADMET studies on the synthesized complexes. The spectroscopic and physical studies showed a change in colour and an increase in melting point due to coordination. The novel compounds were slightly soluble in water. The XRD tests revealed that the new nanocomplexes were crystalline. The Fe (II) nanocomplexes had a size of 57.56 nm and the Cu (II) nanocomplexes had a size of 69.88 nm. These values were found using Debye-Scherrer's equation. The FTIR results of the TMP, Fe (II), and Cu (II) nanometal complexes showed a shift of the amino group band from 3317 to 3295 and 3202 cm^{-1} and the azomethine band from 1633 to 1625 and 1592 cm^{-1} in the complexes. In the complexes, the proton NMR spectra revealed an upfield shift of the amine proton. The carbon-13 NMR spectra showed that CH_2 was involved in coordination with the metal ions. The spectra studies indicated that TMP coordinated with the metal ions through the methylene and amino groups. A trigonal bipyramid structure was proposed for the complexes. The results of the Rule of 5 studies indicated that the test compounds had a good drug-likeness prediction, with only one violation. The ADMET prediction showed that all of the compounds demonstrated improved pharmacokinetic characteristics and adhered to the RO5 requirement. These findings highlight the therapeutic potential of Fe (II) and Cu (II) nano-sized TMP complexes as bioactive compounds that warrant further investigation for pharmaceutical applications.

DOI:10.46481/jnsps.2024.2148

Keywords: Trimethoprim, Fe (II), Cu (II), nano complexes, *in silico*, ADMET

Article History :
Received: 17 May 2024
Received in revised form: 20 June 2024
Accepted for publication: 01 July 2024
Published: 11 July 2024

Communicated by: Emmanuel Etim

1. Introduction

Trimethoprim (TMP) (Figure 1) is a drug that belongs to a group of medicines called diaminopyrimides [1, 2]. This drug stops bacteria from making the dihydrofolate reductase enzyme, which stops dihydrofolate acid (DHF) from changing into tetrahydrofolic acid (THF), which is an active form [3–6]. This could halt thymine production, causing DNA damage. TMP is used equally for both prophylactic and treatment therapy for urinary tract infections [1].

The metal-drug complexes have produced a lot of results [7–15], as neutral metal complexes are more effective against microbes, even those with high levels of drug resistance, when

*Corresponding author Tel. No.: +234-706-292-8066.
Email address: chidonwasogwa@gmail.com (B. C. Asogwa)

compared to the parent drug alone [15]. Various research studies have demonstrated that administering these structurally modified medications, particularly metal complexes, not only has higher pharmacological and toxicological qualities but also exhibits better characteristics [15]. Most transition metals have demonstrated the ability to form stable complexes and exhibit stronger antibacterial properties [7, 8]. This is because they can attach to nucleophilic (electron-rich) substances like DNA and proteins [7, 8].

ADMET research refers to the evaluation of the pharmacokinetics of a drug, encompassing its absorption, distribution, metabolism, excretion, and toxicity. The ADMET study is a crucial component of computational drug design [16]. To select a drug as a therapeutic candidate and advance it into late-stage preclinical and clinical programs, drug developers conduct *in vitro* and *in vivo* research. ADMET qualities are essential for drug researchers to assess the safety and effectiveness of a potential drug, and they are required for regulatory approval [17].

Nanoparticles (NPs) have garnered growing attention across various medical fields due to their capacity to deliver medications within the optimal dosage range, leading to enhanced therapeutic effectiveness, reduced side effects, and improved patient adherence [18, 19]. The surface plasmon resonance (SPR)-enhanced light scattering and absorption of semiconductor and metallic NPs make them highly promising for cancer diagnostics and therapy. The targeted laser photothermal therapy of cancer can effectively utilize Au NPs to convert highly absorbed light into localized heat [20]. The Gd NPs containing several hydroxyl groups exhibited potent antineoplastic activity, demonstrating high efficacy and reduced toxicity [21]. Fe NPs have numerous potential applications, including their use as catalysts, drug delivery platforms, sensors, and for energy storage and conversion [22]. Asogwa *et al.* [23] and Zare *et al.* [24] suggest that probe sonication is a highly efficient method for synthesizing nanomaterials.

The quest for the discovery and synthesis of more efficacious therapies, therapeutic materials, and other tools, as well as devices of lower toxicity than the existing ones, has led us to the development of new nano-sized TMP complexes of Fe (II) and Cu (II). To the best of our knowledge, there are no reports on the synthesis of Fe (II) and Cu (II) in TMP. Furthermore, the Fe(II) and Cu(II) nano-sized complexes of TMP are yet to be reported in the literature. The ADMET studies of these nano-sized complexes have also not been reported. Based on these gaps in the literature, we hereby present the sonochemical synthesis, characterization, and ADMET studies of Fe (II) and Cu (II) nano-sized complexes of TMP.

2. Materials and methods

2.1. Chemicals and solvent

All the reagents used in this study are of analytical grade and were used without further purification.The TMP salt was obtained from Andhra Organics Limited, India. $CuSO_4.5H_2O$ and $FeSO_4.7H_2O$ were obtained from Sigma-Aldrich.

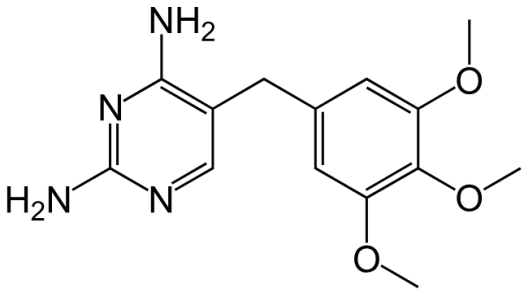

Figure 1. Structure of Trimethoprim.

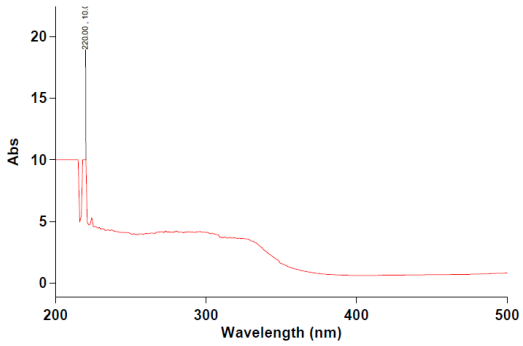

Figure 2. UV/Vis spectrum for TMP.

2.2. Synthesis of Fe (II) and Cu (II) nano-sized complexes of TMP by ultrasonic sonicator method

The nanometal complexes were synthesized following the procedure described by Zare *et al.* [24]. Equimolar (0.1 mole) solutions of TMP (2.90 g) and metal ions (2.78 g of $FeSO_4.7H_2O$ and 1.59 g of $CuSO_4.5H_2O$) each were added together. The mixture was stirred and positioned on an ultrasonic probe of an ultrasonic sonicator that operates at 24 kHz with a maximum force output of 400 W for 30 minutes. The resulting mixture was filtered with a Whatman No. 1. filter paper. The filtrates were then carefully placed in the desiccator to dry. Each of the complexes was stored in a neatly labeled container.

2.3. Physical and spectroscopic analysis

2.3.1. Melting point

Using the Gallenkamp melting point equipment, the melting points (in degrees) of the nanometal complexes were determined. The Gallenkamp apparatus was turned on. The capillary tubes were placed into the oven block and allowed to reach a state of equilibrium for a duration of 1 minute. The temperature was elevated, and the rate of elevation was regulated using the adjustable heat dial. The initial and final temperatures of the sample were recorded.

2.3.2. Solubility test

Different polarity solvents, such as n-hexane, ethanol, water, ethyl acetate, and dimethylsulfoxide, were used to test how well TMP and nanometal complexes could dissolve. Exactly 0.1g of the complex was taken and dissolved into a corresponding 3 mL of the solvents at 25 °C.

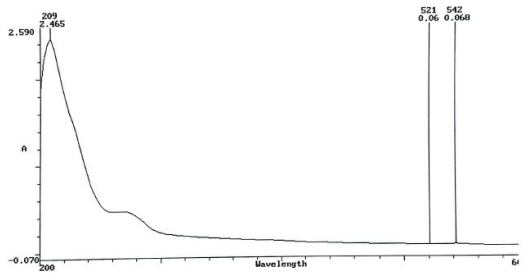

Figure 3. UV/Vis spectrum for $[Fe(TMP)(H_2O)_2]$.

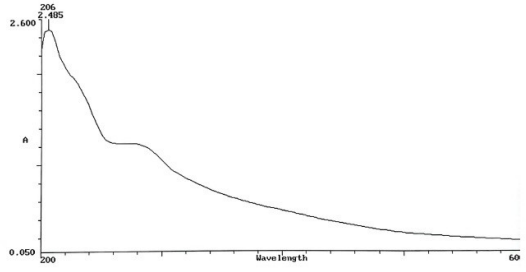

Figure 4. UV/Vis spectrum of $[Cu(TMP)(H_2O)_2]$.

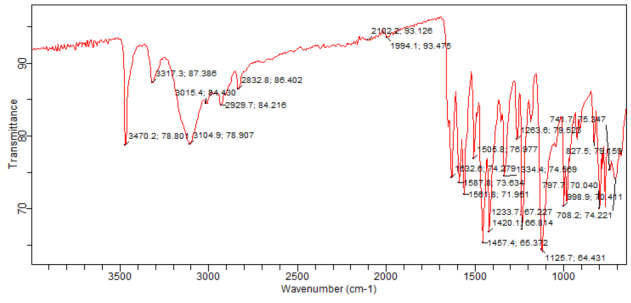

Figure 5. IR spectrum of TMP.

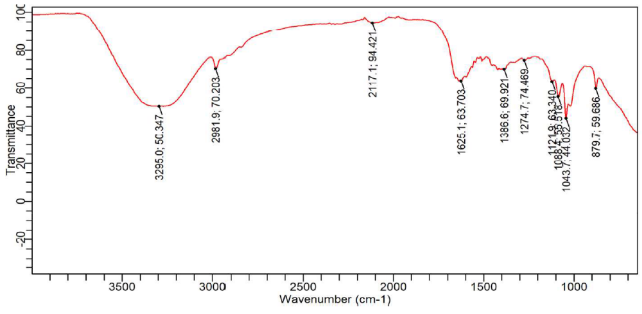

Figure 6. IR spectrum of $[Fe(TMP)(H_2O)_2]$.

2.3.3. *UV/Vis spectroscopy*

The UV/visible spectral measurements of the synthesized nanometal complexes were obtained using a UV-1800 series using dimethoxysulfoxide as solvent. The spectrophotometer was calibrated using distilled water. The cuvette was filled to three-fourths height with the test sample and was scanned from 200 to 800 nm. The display spectra were recorded.

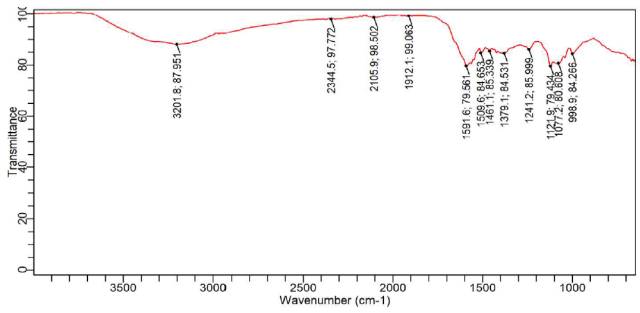

Figure 7. IR spectrum of $[Cu(TMP)(H_2O)_2]$.

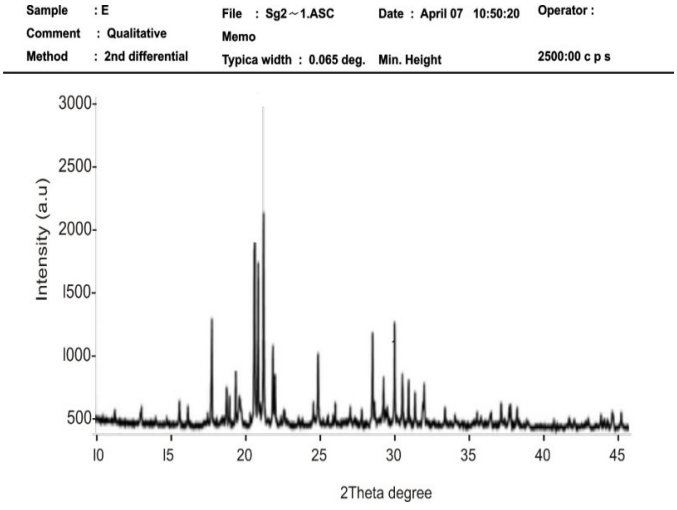

Figure 8. XRD pattern of $[Fe(TMP)(H_2O)_2]$.

2.3.4. *Infrared spectroscopy*

The ligand and nanometal complexes were subjected to FT-IR spectra analysis. IR spectra were obtained using a Perkin Elmer Spectrum BX FT-IR spectrophotometer (4400–600 cm^{-1}) in KBr pellets. Exactly 2 mg of the TMP/complexes were directly deposited onto the KBr plates, followed by the addition of a single drop of DMSO. The prepared sample was inserted into the spectrometer. The FTIR spectrum was obtained by scanning the material throughout a wavelength range of 4000 to 600 cm^{-1}.

2.3.5. *X-ray diffraction*

The pulverized samples were pelletized, sieved to 0.074 mm, and then taken with an aluminum alloy grid (35 mm x 50 mm) on a flat glass plate and covered with paper. Wearing hand gloves, the samples were gently pressed with the hand to become compact and ran through the Rigaku D/Max-lllC X-ray diffractometer. At room temperature, the machine was set to produce diffractions at a scanning rate of 2.0/min in the range of 2 to 500, with CuKa radiation set at 40 kV and 20 mA. The crystallite size of the nanometal complexes was calculated using Debye-Scherrer's equation.

$$D = K\lambda/(\beta cos\theta),$$

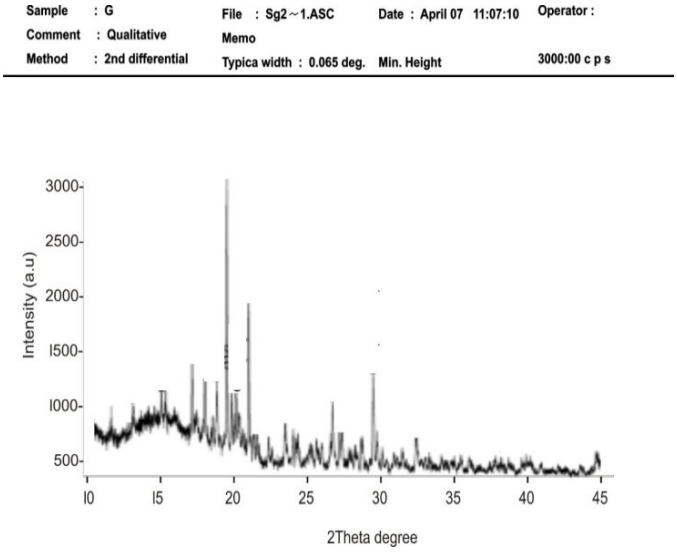

Figure 9. XRD pattern of $[Cu(TMP)(H_2O)_2]$.

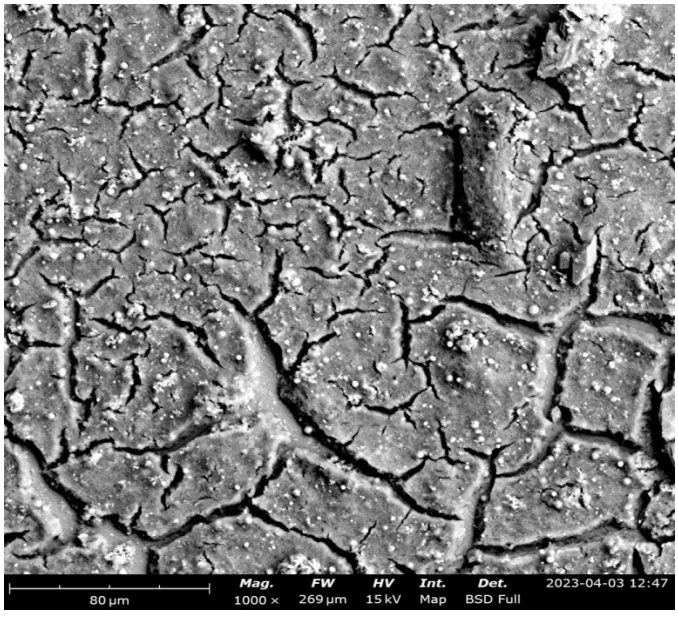

Figure 10. SEM monograph of $[Fe(TMP)(H_2O)_2]$.

where D is the crystallite size of nanoparticles, K is the Scherrer constant = 0.98, λ is wavelength. β is the full width at half maximum (FWHM).

2.3.6. Nuclear magnetic resonance

The NMR spectra measurements were obtained on a Nanalysis X-685 benchtop NMR with a machine frequency of 60 MHz and using deuterated DMSO as solvent. Exactly 5 mg of the sample were dissolved in DMSO-D6 and transferred to the NMR tube. The NMR tube containing the sample was loaded into the NMR spectrometer.

2.3.7. Scanning electron microscope

The morphology and dimensions of silver nanoparticles were analyzed using a German-made scanning electron microscope equipped with EDS-Mapping-Line-EBSD capabilities. The examination was conducted following the placement of the sample in a centrifuge, rotating at a speed of 10,000 rpm for a duration of 15 minutes. Subsequently, the sample was rinsed with distilled water and subjected to drying at a temperature of 50 degrees Celsius. The sample was positioned on a platinum mesh that had been coated with palladium. The analysis of the sample was conducted by examining the radiation that passed through it, resulting in the generation of an image displaying a dispersion spectrum.

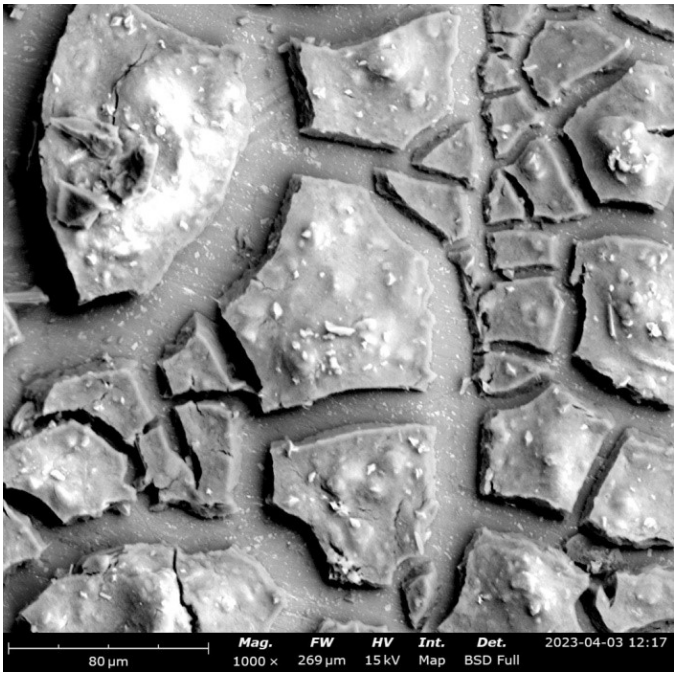

Figure 11. SEM monograph of $[Cu(TMP)(H_2O)_2]$.

Table 1. The solubility profile of TMP and its nanometal complexes.

Compounds	Colour	MP (°C)	% Yield
TMP	white	199	-
$[Fe(TMP)(H_2O)_2]$	brown	210	82
$[Cu(TMP)(H_2O)_2]$	green	220	80

2.4. In-silico studies

2.4.1. ADMET predictions

The ADMET, drug-likeness and interactions were predicted using the Swiss ADME online tool (http://www.swissadme.ch) [25].

2.4.2. Toxicity

The toxicity prediction was done using the ProTox-II online tool (https://tox.charite.de/protox3/index.php?site=compound_input) [26].

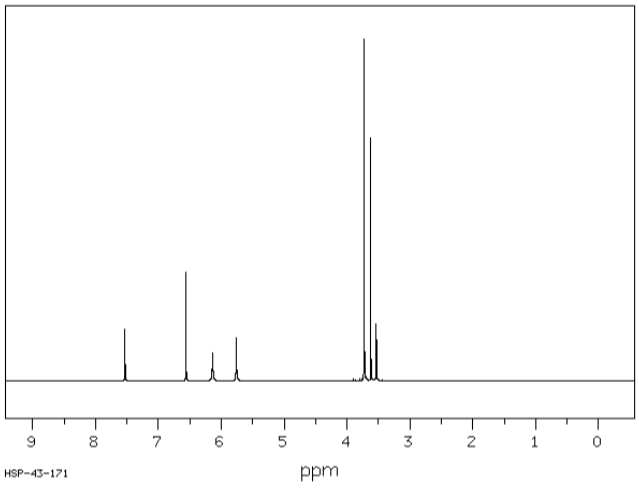

Figure 12. ^{1}H spectrum of TMP [27].

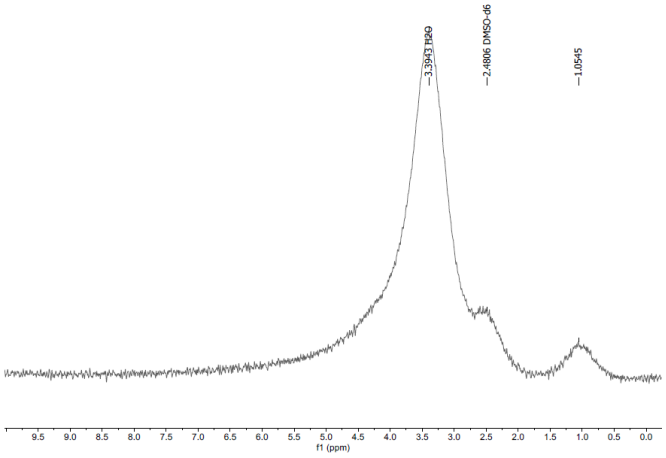

Figure 13. ^{1}H spectrum of [Fe(TMP)$(H_2O)_2$].

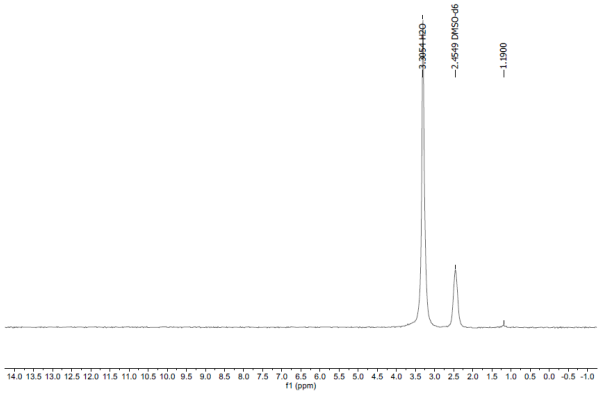

Figure 14. ^{1}H spectrum of [Cu(TMP)$(H_2O)_2$].

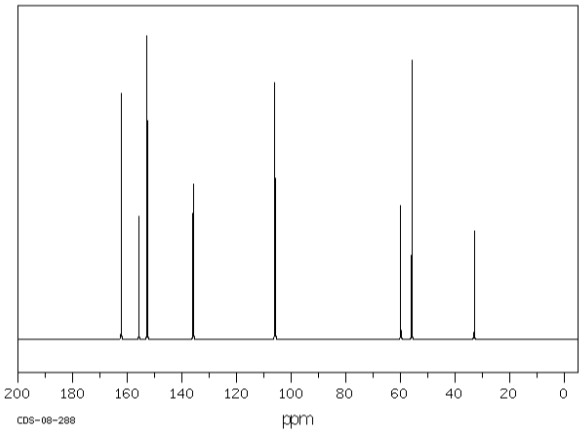

Figure 15. ^{13}C NMR spectrum of TMP [27].

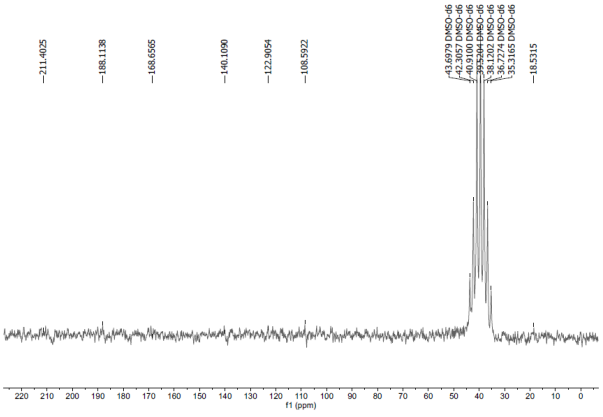

Figure 16. ^{13}C NMR spectrum of [Fe(TMP)$(H_2O)_2$].

3. Results and discussion

3.1. Colour, melting point, and yield (%)

The colour, melting point, and yield (%) are presented in Table 1.

TMP and its nano-metal complexes are crystalline, non-hygroscopic, and air-stable compounds (Table 1). The change in colour suggested that there was a coordination of transition metals with the ligand, as transition metals are known to form coloured compounds [14, 15].

3.2. Solubility

The solubility profile of TMP and its nano-metal complexes is presented in Table 2.

The TMP, Fe(II), and Cu(II) nanocomplexes were observed to be all soluble in ethyl acetate and DMSO solvents (Table 2). This could be attributed to the fact that DMSO and ethylacetate are both known to be polar aprotic solvents because they can dissolve both non-polar and polar compounds in addition to being miscible in different organic solvents [28]. The TMP salt was insoluble in distilled water, while the nano-metal complexes were seen to be slightly soluble in distilled water. The sparing solubility of the complexes in water could be attributed to an increase in polarity.

Table 2. The solubility profile of TMP and its nanometal complexes.

Compounds	*n*-Hexane	Distilled water	Ethanol	Ethyl Acetate	DMSO
TMP	SS	IS	S	S	S
$[Fe(TMP)(H_2O)_2]$	IS	SS	SS	S	S
$[Cu(TMP(H_2O)_2]$	IS	SS	SS	S	S

S = soluble, SS = sparingly soluble, IS = insoluble.

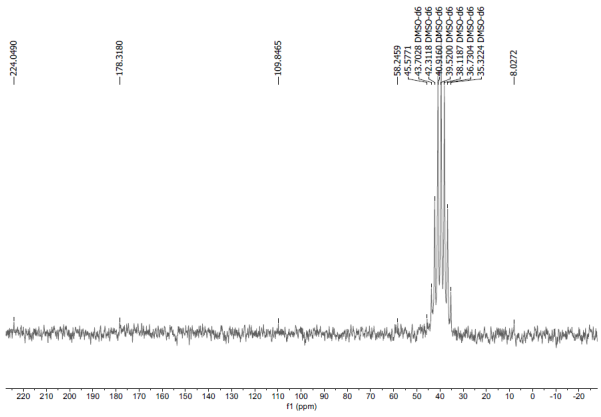

Figure 17. ^{13}C NMR spectrum of $[Cu(TMP)(H_2O)_2]$.

Table 3. Summary of the UV/vis peaks; a comparism of the TMP and its nano metal complexes.

Compounds	Transitions	λ_{max} (nm)
TMP	$n \rightarrow \pi*$	220
$[Fe(TMP)(H_2O)_2]$	$\pi \rightarrow \pi*$	209
	LMCT	300
	$d \rightarrow d$	521, 542
$[Cu(TMP)(H_2O)_2]$	$\pi \rightarrow \pi*$	206
	LMCT	290

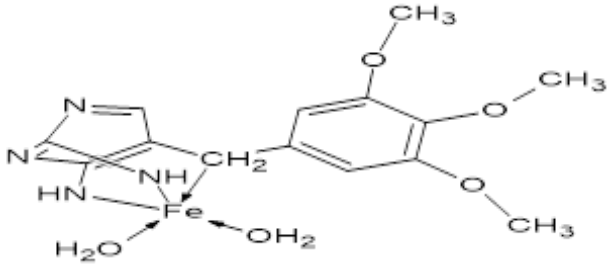

Figure 18. Proposed structure for $[Fe(TMP)(H_2O)_2]$.

3.3. UV/Visible spectroscopy

The summary of the UV/visible spectral data is presented in Table 3, while the spectra are shown in Figures 2, 3, and 4.

The transitions observed at λ = 220, 209 and 206 nm in the UV/vis spectra of TMP and its nanocomplexes (Figures 2, 3 and 4) were assigned to $\pi \rightarrow \pi^*$. These transitions are known as inter-ligand charge transfers (ILCT) (Table 3) [19]. These transitions are due to the chromophores in the test samples. The peaks at 521 and 542 nm in the UV/Vis spectrum for $[Cr(TMP)(H_2O)_2]$ suggested a d-d transition [14, 15]. The d-d transitions indicated the formation of complexes. The peaks at 300 and 290 nm in the UV/Vis spectrum of $[Fe(TMP)(H_2O)_2]$ and $[Cu(TMP)(H_2O)_2]$ were assigned to ligand-to-metal charge transfer (LMCT) [14, 15]. The LMCT implied that the complexes were formed.

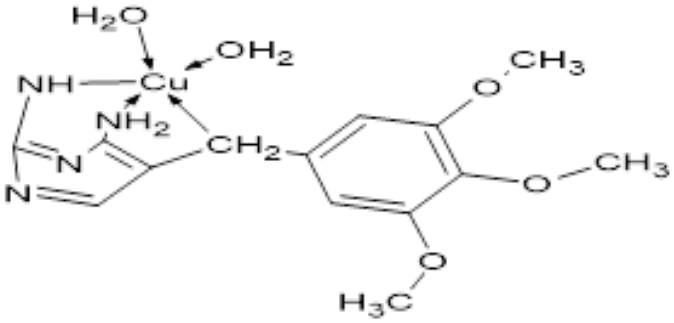

Figure 19. Proposed structure for $[Cu(TMP)(H_2O)_2]$.

3.4. Infrared spectroscopy

Summary of the IR peaks are shown in Table 4. The spectra are presented in Figures 5, 6 and 7.

To elucidate the bonding mechanism and the coordination of the metal ion on the ligand, the FT-IR spectra of the TMP and metal complexes (Table 4) (Figures 5, 6 and 7) were compared and analyzed. TMP has a total of seven potential donor sites: two nitrogen atoms in the pyrimidine rings, two amino groups on the pyrimidine rings, and three methoxy groups. The pyrimidine-NH_2 groups in free TMP have two modes: υas (N H) and υs (N H). These modes are represented by strong and sharp bands at 3470 and 3317 cm^{-1}, respectively. The presence of hydrogen bonds affects these bands [11, 12]. The complexes exhibit bands at υ(N H) in the range of 3295–3202 cm^{-1}, which correspond to asymmetric and symmetric vibrations. These bands show a substantial shift compared to those of the ligand. This suggests that the metal ion is bound to the TMP molecule through the two nitrogen atoms that are part of the NH_2 groups. The vibrational frequency of the C-O-C group remained unchanged in TMP and its complexes. This suggested that coordination did not occur in the methoxy group. The M-O bonds were observed at 880 and 810 cm^{-1} in the complexes.

3.5. XRD

Table 5 presents the summary of XRD spectra data, while Figures 8 and 9 show the diffraction patterns.

The crystallite size of the nanometal complexes was calculated using Debye-Scherrer's equation (Table 5). The crystallite

Table 4. Summary of some IR peaks; a comparison of TMP and its complexes.

Compounds	Absorption bands in cm^{-1}		
	NH_2	C-O-C	M-O
TMP	3470, 3317	1126	Absent
$[Fe(TMP)(H_2O)_2]$	3295	1122	880
$[Cu(TMP)(H_2O)_2]$	3202	1122	810

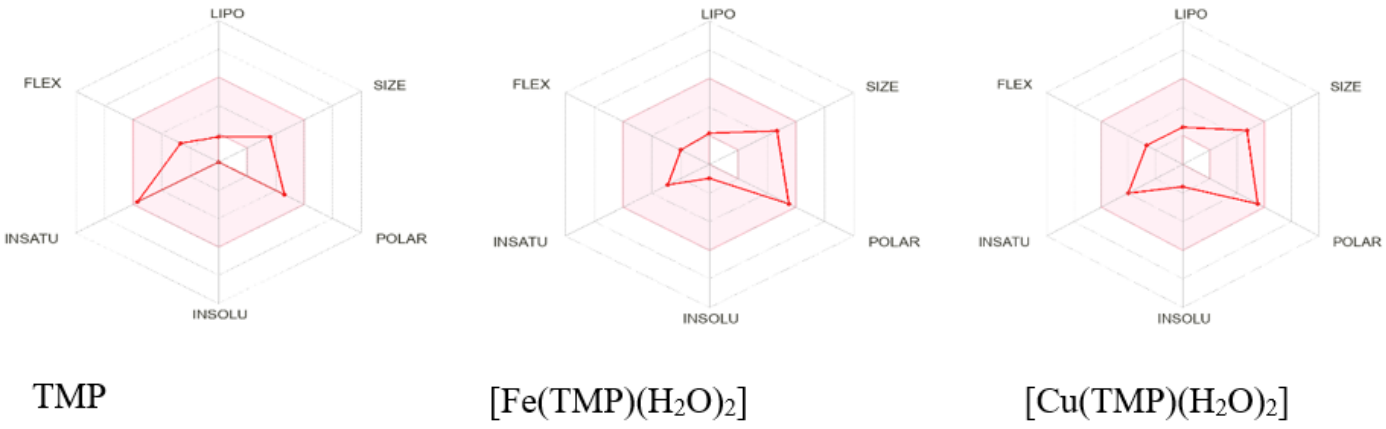

Figure 20. Bioavailability radar of TMP and its nano-sized complexes.

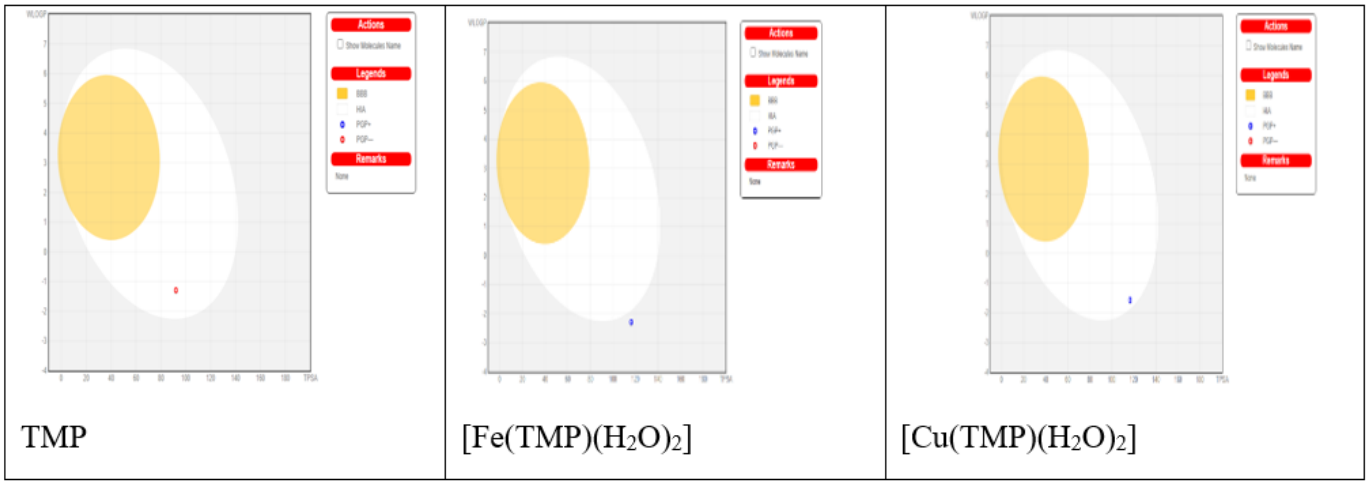

Figure 21. Boiled egg analysis of TMP and its nano-sized complexes.

Table 5. The XRD data showing the 2θ, FWHM, wavelength and crystallite size.

Compound	2θ (^{o})	FWHM (^{o})	λ (nm)	Calculated crystallite size (nm)
$[Fe(TMP)(H_2O)_2]$	37.135	0.164	1.662	57.56
$[Cu(TMP)(H_2O)_2]$	24.653	0.122	1.547	69.88

sizes were 57.56 and 69.88 nm for Fe (II) and Cu (II) nanocomplexes, respectively. The XRD pattern (Figures 8 and 9) also showed that the Fe (II) and Cu (II) nanocomplexes are crystalline.

The SEM monographs of TMP nano-sized complexes are presented in Figures 10 and 11.

3.6. SEM

The SEM monographs (Figures 10 and 11) in this study also revealed that the Fe (II) and Cu (II) nanocomplexes showed a rough, spherical, and compacted structure with porosity and holes to absorb molecules onto the structure.

Table 6. Summary of selected ^{1}H NMR bands; a comparison of the TMP and its complexes.

	Chemical shift (ppm)			
Compounds	H of NH_2	H of CH_2	H of H_2O	Ar-H
TMP	6.14, 5.76	3.53	absent	6.56, 7.53
$[Fe(TMP)(H_2O)_2]$	3.39	1.05	3.39	-
$[Cu(TMP)(H_2O)_2]$	3.30	1.19	3.30	-

Table 7. Summary of selected ^{13}C NMR bands; a comparison of the TMP and its complexes.

	Chemical shift (ppm)	
Compounds	C of CH_2	C of C=C
TMP	32.92	105.00
$[Fe(TMP)(H_2O)_2]$	18.53	108.59
$[Cu(TMP)(H_2O)_2]$	8.03	109.85

3.7. NMR

The ^{1}H NMR spectral data are depicted in Table 6. The spectra are shown in Figures 12, 13 and 14.

The ^{13}C NMR spectral data are depicted in Table 7. The spectra are shown in Figures 15, 16 and 17.

The ^{1}H NMR spectrum of TMP (Figure 12) showed a singlet peak at 3.53 ppm, which corresponded to the proton on CH_2. This chemical shift was observed upfield in the ^{1}H NMR spectrum of the nanometal complexes (Table 6) (Figures 13 and 14), showing coordination with a metal atom. The protons of the NH_2 group were observed at 6.14 and 5.76 ppm in the ligand spectrum. These peaks shifted upfield in the spectrum of the nanometal complexes owing to coordination with the metal ion [11, 12]. The presence of protons of H_2O was observed at 3.39 and 3.30 ppm in the spectrum of the Fe(II) and Cu(II) nano-sized complexes of TMP.

A comparison of the ^{13}C spectra of TMP and its nanometal complexes (Table 7) (Figures 15, 16 and 17) showed that the carbon of CH_2 was observed at 32.92 ppm, while the carbon of CH_2 of the Fe(II) and Cu(II) nano-sized complexes were observed at 18.53 and 8.03 ppm, respectively. This shift suggests that coordination occurs through the CH_2 group.

Based on the spectroscopic study, the proposed structures in Figures 18 and 19 have been proposed for the Fe (II) and Cu(II) nanocomplexes.

3.8. In silico studies

3.8.1. Drug-likeness prediction

The Lipinski Rule of 5 (RO5) is a guideline established by Lipinski *et al.* [29] to assess if a molecule with a specific bioactivity possesses the necessary physical and chemical properties to be an effective oral medicine. According to Lipinski's rule, an oral drug should typically not exceed one violation of the following criteria: The maximum number of hydrogen bond donors should not exceed 5. The maximum number of hydrogen bond acceptors allowed is 10. A molecular mass below 500 daltons. The Clog P value should be less than or equal to 5, indicating the octanol-water partition coefficient. The molar refractivity should range from 40 to 130.

The drug-likeness prediction (Table 8) indicated that there was one violation out of five for the test compounds. These findings indicate that TMP and its complexes meet RO5 standards. Predictions indicate a low attrition rate for the ligand and nanocomplexes, indicating their suitability for further drug development studies [30].

3.9. ADMET predictions

The ADMET predictions are presented in Table 9.

Lipinski *et al.* [28] state that the topological polar surface area (TPSA) is a crucial chemical descriptor that strongly relates to pharmacokinetic features. A desirable drug should have a TPSA value below 140 Å^2. The TPSA values of the test compounds, as shown in Table 9, are below 140 Å^2, indicating that they are likely to be effective medications. The presence of a soluble molecule greatly simplifies certain drug development tasks, particularly in terms of handling and formulation. In addition, solubility is a significant factor that affects absorption in discovery programs focused on oral delivery. In addition, a medicine intended for parenteral administration must have high solubility in water in order to effectively deliver a significant amount of the active component within the limited volume of the pharmaceutical dosage. The water solubility profile for the test chemicals has been provided using the estimated solubility (ESOL) model (Table 9). The solubility profile indicated that TMP was not soluble, whereas the complexes were soluble. The test compounds exhibit a favorable bioavailability score between 0.55 and 0.85. In order for a chemical to be deemed a therapeutic candidate, it typically needs to have a minimum bioavailability score of 0.10 [31]. This indicates that all the test substances are expected to be able to be absorbed and utilized by the body when taken orally. PAINS, short for pan assay interference compounds, are chemicals that exhibit strong activity in tests regardless of the specific protein target. They are sometimes referred to as frequent hitters or promiscuous compounds. The findings of our study indicate that there are no chemicals with promiscuous properties that can potentially create medication interference. The score for synthetic accessibility is normalized on a scale of 1 (indicating easy synthesis) to 10 (indicating highly difficult synthesis). The synthetic accessibility test score of the test compounds (Table 9) indicates that the test compounds can be readily synthesized.

3.9.1. Enzyme-interaction prediction

The enzyme-interaction prediction with cytochromes P450 are presented in Table 10.

The inhibition of these isoenzymes is a significant factor in drug-drug interactions that affect pharmacokinetics. This inhi-

Table 8. Drug-likeness prediction.

Compounds	Mol. Weight	HB Acceptor	HB Donor	Lipophilicity LogP (g/mol)	Molar refractivity	No of violations
TMP	290.32	5	2	2.32	85.98	1 WLOGP<-0.4
$[Fe(TMP)(H_2O)_2]$	384.21	9	6	0.00	94.82	1 WLOGP<-0.4
$[Cu(TMP)(H_2O)_2]$	388.89	9	5	0.00	95.86	1 WLOGP<-0.4

Table 9. ADMET Parameters prediction.

Compound	TPSA (Å²)	Water Solubility Log *S* (ESOL)	Bio. Avail. Score	Med. Chem. (PAIN)	Synthetic Accessibility
TMP	92.09	0.14	0.55	0	4.71
$[Fe(TMP)(H_2O)_2]$	116.27	-1.92	0.55	0	6.53
$[Cu(TMP)(H_2O)_2]$	116.60	-1.57	0.55	0	5.72

Table 10. Interactions with cytochromes P450 (CYP).

Compounds	CYP1A2	CYP2CP	CYP2D6	CYP3A4	Log K_p(skin permeation)(cm/s)
TMP	No	No	No	No	-9.77
$[Fe(TMP)(H_2O)_2]$	No	No	No	No	-9.84
$[Cu(TMP)(H_2O)_2]$	No	No	No	No	-9.35

bition can cause the drug or its metabolites to build up, resulting in hazardous or undesirable side effects due to reduced clearance. Therefore, it is crucial for drug discovery to accurately predict the likelihood of a compound causing substantial drug interactions by inhibiting CYPs, as well as identify the specific isoforms that are impacted. The synthesized nanometal complexes and the ligand (TMP) demonstrated no inhibitory effect on any of the five isoenzymes (CYP1A2, CYP2C19, CYP2C9, CYP2D6, CYP3A4) (Table 10). Based on their negative log Kp values, all the test substances were anticipated to be non-permeable to the skin. Potts & Guy [32] demonstrated that there is an inverse relationship between the log Kp (with Kp measured in cm/s) and the permeability of the molecule through the skin. In other words, the more negative the log Kp value, the lower the molecule's permeability. All chemicals have negative log Kp values. This indicates that TMP and its nano-sized complexes do not permeate the skin.

3.9.2. *Bioavailability radar and boiled egg*

The bioavailability radar of the ligands and nano metal complexes are presented in Figure 20 while the BOILED Egg analysis is presented in Figure 21.

The Bioavailability Radar (Figure 20) is presented to quickly assess the drug-likeness of the ligand and complexes. When considering the qualities of the substances, six physicochemical factors were considered: lipophilicity, size, polarity, solubility, flexibility, and saturation. Descriptors taken from Ritchie *et al.* [33] were used to create a physicochemical range on each axis. The molecule must completely fall within the pink area of the radar plot in order to be classified as drug-like. The bioavailability radar prediction indicated that both the ligand and the nanometal complexes possess six properties, namely lipophilicity, flexibility, size, polarity, insaturation, and insolubility, which fall within the suggested range for a prospective drug. The BOILED-Egg (Figures 11) provides a straightforward method for assessing human gastrointestinal absorption (HIA) and blood-brain barrier (BBB) based on the molecular position in the WLOGP-versus-TPSA reference system. The white zone indicates a high likelihood of passive absorption by the gastrointestinal tract, while the yellow region (yolk) indicates a high likelihood of brain penetration. The yolk and white portions are not mutually exclusive [33]. Furthermore, the points are highlighted in blue if they are anticipated to be actively expelled by permeability glycoprotein, P-gp (PGP+), and in red if they are projected to be non-substrates of P-gp (PGP−). The ligand (TMP) had a red dot within the white area, suggesting that it is not a substrate of permeability glycoprotein (PGP−). In contrast, the nanometal complexes exhibited blue-colored dots, indicating their active efflux by P-gp (PGP+). The Fe (II) nanocomplex was determined to exhibit no absorption of the HIA due to its location outside the region corresponding to a BOILED egg; however, the Cu (II) nanocomplex showed absorption in the HIA since it was situated within the white region of the BOILED egg diagram.

3.9.3. *Toxicity studies*

ProTox-II was used to assess the *in silico* toxicity of the TMP and its nanocomplexes (Table 11). Nwankwo *et al.* [34] and Otuokere *et al.* [35] have used this server to determine toxicity. The Fe (II) nanocomplex is predicted to belong to a higher toxicity class of IV (harmful if swallowed, $300 < LD_{50} \leq 2000$ mg/kg), while the ligand and the Cu (II) nanocomplex were predicted to belong to class III based on their LD_{50} (toxic if swallowed, $50 < LD_{50} \leq 300$ mg/kg). This LD_{50} value is a prediction value of toxic dosage in mg/kg, giving the median lethal dose. Iron complexation reduced the drug's toxicity.

Table 11. Toxicity information of TMP and its nano metal complexes.

Compounds	Predicted LD_{50} (mg/kg)	Predicted Toxicity Class	Average similarity: (%)	Prediction Accuracy: (%)
TMP	187	III	31.61	23
$[Fe(TMP)(H_2O)_2]$	500	IV	27.48	12
$[Cu(TMP)(H_2O)_2]$	300	III	32.39	23

4. Conclusion

The synthesis and characterization of nanocomplexes of Fe (II) and Cu (II) with TMP were conducted. The nanometal complexes were synthesized by the sonication method and characterized based on the observed FTIR spectra, electronic spectra, melting temperature, solubility, proton NMR, and carbon-13 NMR. With a crystallite size of 76.08 nm and 37.13 nm, the XRD pattern showed that the Fe (II) and Cu (II) nanocomplexes are crystalline. The complexes were suggested to have a trigonal bipyramid structure. The *in silico* experiments revealed that the test compounds exhibit favorable predictions in terms of drug-likeness, TPSA value, synthetic accessibility, water solubility, skin permeability, and bioavailability score. The toxicity prediction indicated that TMP toxicity was decreased through complexation with iron. The study's findings and conclusions show that the TMP nano-sized complexes have a wide range of ADMET profiles, which means they are safe and could be used for therapeutic purposes. These findings necessitate further investigation into their in vivo, pre-clinical, and clinical studies. Future research should prioritize investigating the fundamental processes behind the therapeutic benefits and conducting clinical trials to confirm their effectiveness and safety in humans.

References

[1] A. Abeer & S. R. Moamen, "Synthesis, spectroscopic characterizations and biological studies on Gold(III), Ruthenium(III) and Iridium(III) complexes of trimethoprim antibiotic drug", Bulletin of the Chemical Society of Ethiopia **38** (2024) 701. https://www.ajol.info/index.php/bcse/article/view/266832.

[2] F. M. Ibrahim, R. A. Hammza & D. H. Fadhil, "Synthesis and characterization f Trimethoprim metal complexes used as corrosion inhibitors for carbon steel in acid media", International Journal of Corrosion and Scale Inhibition **8** (2019) 733. .

[3] M. Salehi, H. Shariatifar, J. M. G. Ghanbari & A. Farasat, "A comprehensive study of human serum albumin interaction with trimethoprim using molecular docking and molecular dynamics methods: an appropriate tool for drug delivery systems", Journal of Inflammatory Diseases **25** (2021) 99. .

[4] A. Wróbel & D. Drozdowska, "Recent design and structure-activity relationship studies on modifications of dhfr inhibitors as anticancer agents", Current Medicinal Chemistry **26** (2019) 1. https://www.ingentaconnect.com/content/ben/cmc/2021/00000028/00000005/art00004.

[5] A. Wróbel, K. Arciszewska & D. Maliszewski, "Trimethoprim and other nonclassical antifolates an excellent template for searching modifications of dihydrofolate reductase enzyme inhibitors", The Journal of Antibiotics **73** (2020) 5. https://www.nature.com/articles/s41429-019-0240-6.

[6] H. Juan, Q. Wenliang, A. Qi, Y. Tao & L. Youfu, "Dihydrofolate reductase inhibitors for use as antimicrobial agents", European Journal of Medicinal Chemistry **195** (2020) 112268. https://www.sciencedirect.com/science/article/abs/pii/S022352342030235X.

[7] O. Ugochukwu & I. E. Otuokere, "Synthesis, spectroscopic characterization and antibactrial activities of Co (II) complex of ofloxacin drug mixed with ascorbic acid as a secondary ligand", BioScientific Review **3** (2021) 1. https://doi.org/10.32350/BSR.0303.01.

[8] I. E. Otuokere, U. F. Robert, K. K. Igwe & S. U. Mpama, "Synthesis, characterization and antibacterial studies of benzylpenicillin and its Co(II) Complex", ChemSearch Journal **11** (2020) 9. https://www.ajol.info/index.php/csj/article/view/197367.

[9] I. E. Otuokere, J. G. Ohwimu, K. C. Amadi, C. O. Alisa, F. C. Nwadire, O. U. Igwe, A. A. Okoyeagu & C. M. Ngwu, "Synthesis, characterization and molecular docking studies of Mn (II) complex of sulfathiazole", Journal of the Nigerian Society of Physical Sciences **1** (2019) 95. https://doi.org/10.46481/jnsps.2019.20.

[10] I. O. Edozie, O. J. Godday, A. K. Chijioke, I. O. Uchenna & N. F. Chigozie, "Synthesis, characterization and molecular docking studies of Co (II) metal complex of sulfathiazole", Bulletin of the Chemical Society of Ethiopia **34** (2020) 83. https://www.ajol.info/index.php/bcse/article/view/195192.

[11] I. E. Otuokere, U. F. Robert & K. K. Igwe, "Chelating and antibacterial potentials of benzylpenicillin and its Ni (II) complex", Communication in Physical Sciences **8** (2022) 138. https://journalcps.com/index.php/volumes/article/view/269.

[12] I. E. Otuokere, J. C. Anyanwu & K. K. Igwe, "Synthesis, characterization and antibacterial studies of 4-{[(E)- Phenylmethylidene]amino}-N-(1,3-thiazol-2-yl)benzenesulfonamide and its Mn(II) Complex", Chemsearch Journal **11** (2020) 44. https://www.ajol.info/index.php/csj/article/view/197378.

[13] I. E. Otuokere, K. C. Nwaiwu, F. C. Nwadire & O. U. Akoh, "Synthesis and characterization of Cr (III)-ascorbic acid complex", Journal of Applied Sciences and Environmental Management **26** (2022) 75. https://www.ajol.info/index.php/jasem/article/view/222637.

[14] I. E. Otuokere, L. O. Okpara, K. C. Amadi, N. Ikpo, G. U. Okafor & F. C. Nwadire,"Synthesis, characterization and complexation of Cr(III) ion using chloroquine diphosphate drug", Journal of Chemical Society of Nigeria **44** (2019) 107. https://journals.chemsociety.org.ng/index.php/jcsn/article/view/254.

[15] I. E. Otuokere & U. F. Robert, "Synthesis, characterization and antibacterial studies of (3, 3-Dimethyl-7-oxo-6-(2-phenylacetamido)-4-thia-1-azabicyclo [3.2. 0]heptane-2-carboxylic acid-Cr (III) Complex", Journal of Nepal Chemical Society **41** (2020) 1. https://doi.org/10.3126/jncs.v41i1.30370.

[16] N. Flores-Holguín, J. Frau & D. Glossman-Mitnik,"Computational pharmacokinetics report, ADMET study and conceptual DFT-based estimation of the chemical reactivity properties of marine cyclopeptides", Chemistry Open **10** (2021) 1142. https://www.ncbi.nlm.nih.gov/pmc/articles/PMC8607802/.

[17] L. L. G. Ferreira & A. D. Andricopulo, "ADMET modeling approaches in drug discovery", Drug discovery today **24** (2019) 1157. https://doi.org/10.1016/j.drudis.2019.03.015.

[18] I. Khan, K. Saeed & I. Khan, "Nanoparticles: properties, applications and toxicities", Arabian Journal of Chemistry **12** (2019) 908. https://doi.org/10.1016/j.arabjc.2017.05.011.

[19] A. F. Burlec, A. Corciova, M. Boev, D. Batir-Marin, C. Mircea, O. Cioanca, G. Danila, M. Danila, A. F. Bucur & M. Hancianu, "Current overview of metal nanoparticles' synthesis, characterization, and biomedical applications, with a focus on silver and gold nanoparticles", *Pharmaceuticals* ***16*** (2023) 1410. https://doi.org/10.3390/ph16101410.

[20] O. Afzal, A. S. A. Altamimi, M. S. Nadeem, S. I. Alzarea, W. H. Almalki, A. Tariq, B. Mubeen, B. N. Murtaza, S. Iftikhar, N. Riaz & I. Kazmi, "Nanoparticles in drug delivery: from history to therapeutic applications", Nanomaterials **12** (2022) 4494. https://doi.org/10.3390/nano12244494.

[21] T. M. Joseph, D. Kar Mahapatra, A. Esmaeili, L. Piszczyk, M. S. Hasanin, M. Kattali, J. Haponiuk & S. Thomas, "Nanoparticles: taking a unique position in medicine", Nanomaterials **13** (2023) 574. https://doi.org/10.3390/nano13030574.

[22] N. Zahin, R. Anwar, D. Tewari, M. T. Kabir, A. Sajid, B. Mathew, M. S. Uddin, L. Aleya & M. M. Abdel-Daim, "Nanoparticles and its biomedical applications in health and diseases: special focus on drug delivery", Environmental science and pollution research international **27** (2020) 1915. https://link.springer.com/article/10.1007/s11356-019-05211-0.

[23] B. C. Asogwa & I. E. Otuokere, "Sonochemical synthesis and characterization of Fe(II) and Cu(II) nano-sized complexes of sulfamethoxazole", Journal of the Nigerian Society of Physical Sciences **6** (2024) 2011. https://journal.nsps.org.ng/index.php/jnsps/article/view/2011.

[24] N. Zare, A. Zabardasti & A. Mohammadi, "Sonochemical synthesis, characterization, biological applications, and DFT study of new nano-sized manganese complex of azomethine derivative of diaminomaleonitrile", Journal of Iran Chemical Society **16** (2019) 1501. https://doi.org/10.1007/s13738-019-01626-1.

[25] Swiss Institute of Bioinformatics, (2024). https://www.sib.swiss/.

[26] ProTox-II: a web server for the prediction of toxicity of chemicals. https://academic.oup.com/nar/article/46/W1/W257/4990033.

[27] Spectral Database for Organic Compounds (SDBS) | UCSB library, National institute of advanced industrial science and tecnology, Japan. https://www.library.ucsb.edu/spectral-database-organic-compounds-sdbs.

[28] S. Sarala, S. K. Geetha, S. Muthu & A. Irfan, "Theoretical investigation on influence of protic and aprotic solvents effect and structural (Monomer, Dimer), Van-der Waals and Hirshfeld surface analysis for clonidine molecule", Computational and Theoretical Chemistry **1204** (2021) 113397. https://doi.org/10.1016/j.comptc.2021.113397.

[29] C. A. Lipinski, F. Lombardo, B. W. Dominy & P. J. Feeney, "Experimental and computational approaches to estimate solubility and permeability in drug discovery and development settings", Advanced Drug Delivery Reviews **23** (1997) 3. https://doi.org/10.1016/S0169-409X(96)00423-1.

[30] I. E. Otuokere, O. U. Akoh, J. O. Echeme, F. C. Nwadire, C. I. Nwankwo, J. N. Egbucha & K. Ammasai, "GC-MS analysis and molecular docking studies to identify potential SARS-CoV-2 nonstructural protein inhibitors from *Icacina trichantha* Oliv Tubers", Tropical Journal of Natural Product Research **6** (2022) 1342. https://www.cabidigitallibrary.org/doi/full/10.5555/20220411245.

[31] Y. C. Martin, "A bioavailability score", Journal of Medicinal Chemistry **48** (2005) 3164. https://pubs.acs.org/doi/abs/10.1021/jm0492002.

[32] R. O. Potts & R. H. Guy, "Predicting skin permeability", Pharmaceutical Research **09** (1992) 663. https://link.springer.com/article/10.1023/A:1015810312465.

[33] T. J. Ritchie, P. Ertl & R. Lewis, "The graphical representation of ADME-related molecule properties for medicinal chemists", Drug Discovery Today **16** (2011) 65. https://www.sciencedirect.com/science/article/abs/pii/S1359644610008056.

[34] C. I. Nwankwo, T. N. Omeh, O. D. Omodamiro, I. E. Otuokere, P. O. Alaebo, O. C. Atasie & G. A. Ekwuribe, "Phenolics of pods: hplc identification *and in silico* studies to identify potential anti-inflammatory agents", Tropival Journal of Natural Product Research **6** (2022) 1311. https://www.cabidigitallibrary.org/doi/full/10.5555/20220411242.

[35] I. E. Otuokere, O. U. Akoh, F. C. Nwadire, C. I. Nwankwo, J. N. Egbucha, C. Wisdom & O. A. Okwudiri, "GC-MS profiling and in silico studies to identify potential sars-cov-2 nonstructural protein inhibitors from *Psidium guajava*", African Scientific Reports **1** (2022) 161. https://asr.nsps.org.ng/index.php/asr/article/view/52.